Charge Transport Modulation of a Flexible Quantum Dot Solar Cell Using a Piezoelectric Effect

Yuljae Cho, Paul Giraud, Bo Hou, Young-Woo Lee, John Hong, Sanghyo Lee, Sangyeon Pak, Juwon Lee, Jae Eun Jang, Stephen M. Morris, Jung Inn Sohn, SeungNam Cha,* and Jong Min Kim*

Colloidal quantum dots are promising materials for flexible solar cells, as they have a large absorption coefficient at visible and infrared wavelengths, a band gap that can be tuned across the solar spectrum, and compatibility with solution processing. However, the performance of flexible solar cells can be degraded by the loss of charge carriers due to recombination pathways that exist at a junction interface as well as the strained interface of the semiconducting layers. The modulation of the charge carrier transport by the piezoelectric effect is an effective way of resolving and improving the inherent material and structural defects. By inserting a porous piezoelectric poly(vinylidenefluoride-trifluoroethylene) layer so as to generate a converging electric field, it is possible to modulate the junction properties and consequently enhance the charge carrier behavior at the junction. This study shows that due to a reduction in the recombination and an improvement in the carrier extraction, a 38% increase in the current density along with a concomitant increase of 37% in the power conversion efficiency of flexible quantum dots solar cells can be achieved by modulating the junction properties using the piezoelectric effect.

Flexible solar cells have emerged as promising energy sources for a variety of advanced technological applications such as electronic textiles, artificial skin, and portable devices. This is because solar cells that are conformable can be easily integrated into various shapes and surfaces.[1,2] To date, considerable effort has already been devoted to realizing high efficiency flexible solar cells. As an example, a recent development has been the demonstration of solution processible light absorption materials as well as highly flexible and stretchable electrodes that maintain the device performance on the application of strain/stress.[3–8] To further advance current flexible solar cell technologies, however, a larger absorption efficiency is required so as to have a high solar cell efficiency with a photoactive layer that is as thin as possible in order to attain a high degree of flexibility. In this regard, colloidal quantum dots (QDs) are one of the most promising materials as they have been shown to exhibit a high light absorption coefficient, a tunable band gap across the solar spectrum, and are solution processible.[9,10]

Among the various types of QD materials, lead sulfide (PbS) QDs are considered to be one of the most attractive materials for solar cell applications because of their large Bohr radius, wide tuning range of the band gap, low material cost, and air stability.[11] As a result of these properties, PbS QD solar cells (QDSCs) have demonstrated a remarkable improvement in the efficiency when used in conventional, rigid solar cell architectures.[12] However, there is still room for further improvement in the QDSC performance. For example, by addressing factors such as the relatively low built-in potential, the excessive surface trap sites and interfaces, which cause an open circuit voltage (V_{oc}) deficit, and the low charge carrier dissociation and collection rate, it has been possible to enhance the performance of the solar cells.[13–16] In particular, the heterojunction between the electron transport layer (ETL) and the PbS QD layer plays a key role in governing the overall performance of the PbS QDSCs because charge trapping and recombination occurs much faster at this heterojunction than at other locations between and within the PbS QD layers.[17] To reduce the charge recombination at the interfaces, various strategies have been considered, such as engineering the energy band levels as well as the employment of a buffer layer.[18–20] However, flexible QDSCs are more susceptible to the loss of charge carriers at the junction due to recombination pathways that arise from the straining of the semiconducting layers during the fabrication process, which is a major limitation that has to be dealt with for an improvement in the performance of flexible QDSCs to be realized.[9,10] Therefore, fundamental strategies for structurally and actively controlling the junction properties are required to boost extraction and reduce the recombination of

Y. Cho, P. Giraud, Dr. B. Hou, Dr. Y.-W. Lee, J. Hong, Dr. S. Lee, S. Pak, J. Lee, Prof. S. M. Morris, Dr. J. I. Sohn, Prof. S. Cha
Department of Engineering Science
University of Oxford
Parks Road, Oxford OX1 3PJ, UK
E-mail: junginn.sohn@eng.ox.ac.uk; seungnam.cha@eng.ox.ac.uk
Prof. J. E. Jang
Department of Information and Communication Engineering
Daegu Gyeongbuk Institute of Science and Technology
Daegu 711-873, Republic of Korea
Prof. J. M. Kim
Department of Engineering
University of Cambridge
9 JJ Thomson Avenue, Cambridge CB3 0FA, UK

DOI: 10.1002/aenm.201700809

photogenerated charges in order to advance the performance of flexible QDSCs.

Toward this end, we have employed a porous piezoelectric poly(vinylidenefluoride-trifluoroethylene) (P(VDF-TrFE)) polymer layer between a zinc oxide (ZnO) ETL and a PbS QD heterojunction in a flexible QDSC. Through the active control of strain/stress of the flexible form factors, the inserted porous P(VDF-TrFE) layer generates a piezoelectric potential which modulates the junction properties and consequently changes the behavior of the charge carriers. As a result, the modulated electric field at the junction effectively extracts the photogenerated charges and reduces radiative recombination, resulting in enhanced current density (J_{sc}) and consequently a higher power conversion efficiency (PCE) in the flexible solar cells.

Figure 1a shows a schematic structure and photographs of the flexible PbS QDSCs that were treated with tetrabutylammonium iodide (TBAI) and 1,2-ethanedithiol (EDT) ligands.[12,21] The absorption peak and high resolution transmission electron microscopy (HRTEM) analysis revealed that the band gap of the PbS QDs was 1.23 eV and the QDs showed the typical rock-salt cubic characteristics as indicated by the indexed lattice fringes ((200) and (100)) in Figure 1b, respectively. A P(VDF-TrFE) layer was inserted between the ZnO ETL and the PbS QD layers so as to modulate the junction properties by introducing a piezoelectric potential. Further details of the solar cell fabrication method are provided in the Experimental Section. In spite of the high piezoelectric coefficient and flexibility of the P(VDF-TrFE) film, the insulating nature of the polymer restricts efficient transport of the charge carriers. The use of a conjugated structure, which was a mixture of a semiconducting material with the polymer, has been reported previously. However, it was noted that the diverging and nonuniform electric field that was caused by the randomly distributed P(VDF-TrFE) polymer limited the efficient dissociation and extraction of the charge carriers.[22–24] In order to generate a converging and uniform electric field together with secured charge carrier paths, a P(VDF-TrFE) layer with a porous structure was deposited on top of the ZnO ETL as shown by the atomic force microscopy (AFM) image in Figure 1c (left). Afterward, the porous P(VDF-TrFE) layer was thermally annealed to form a piezoelectric β-phase as shown in Figure 1c (top right) which exhibits the most favorable piezoelectric properties in comparison to the other phases of

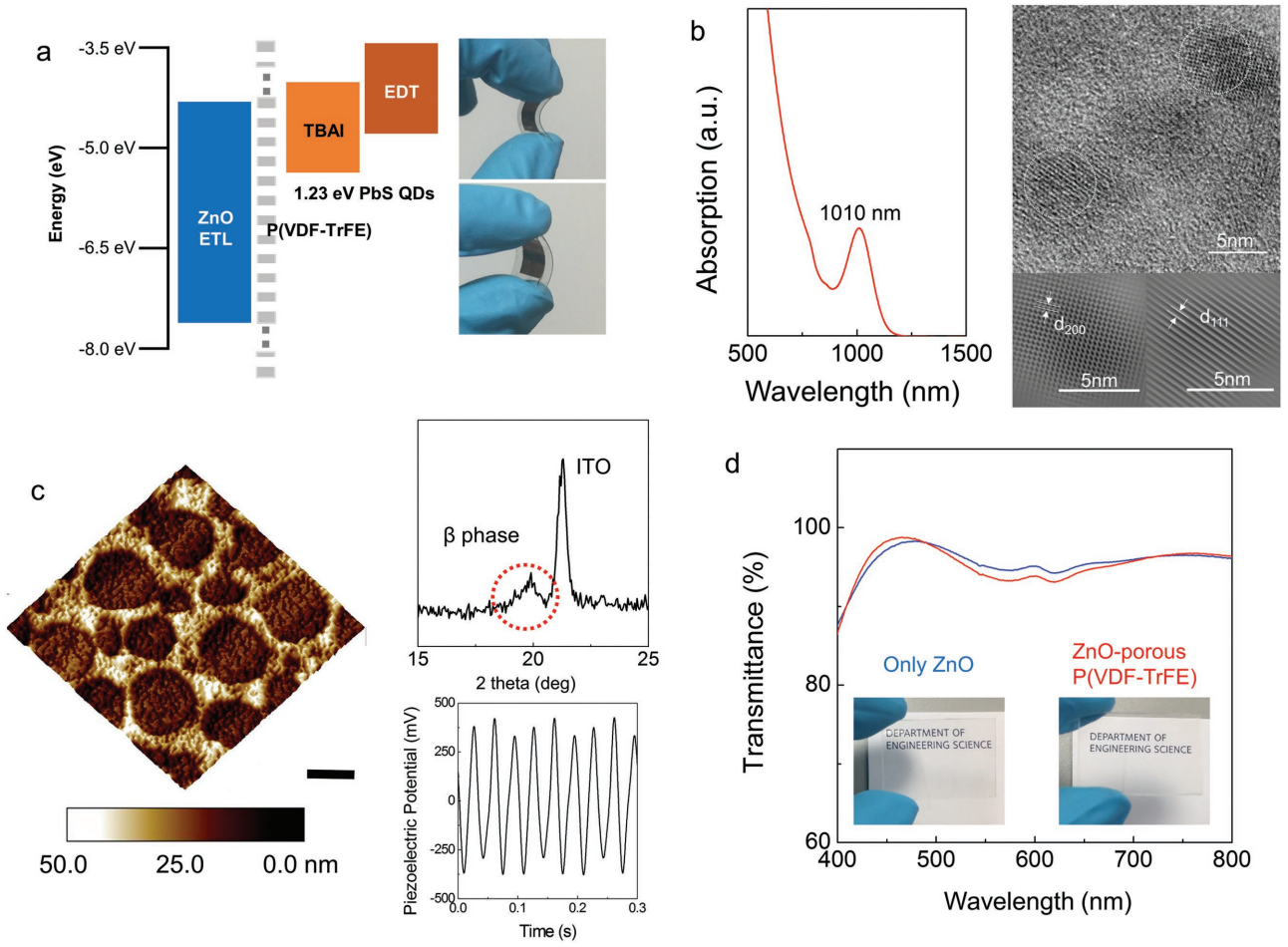

Figure 1. a) Energy structure and photographs of the flexible PbS QDSC. b) Absorption peak of the synthesized PbS QDs and corresponding TEM (and HRTEM) images. c) AFM image of a porous-structured P(VDF-TrFE) film at a scan size of 10×10 μm^2 (scale bar: 2 μm), the formation of the β-phase P(VDF-TrFE) film measured by XRD (top right), and the generation of a piezoelectric potential by the flexible PbS QDSC (bottom right). d) Transmittance of only ZnO (blue) and ZnO-porous P(VDF-TrFE) ETL (red).

P(DF-TrFE) polymers.[25,26] The β-phase P(VDF-TrFE) layer in the flexible PbS QDSC generated a piezoelectric potential under mechanical vibration at a frequency of 30 Hz as shown in Figure 1c (bottom right and Figure S1, Supporting Information). In addition, the transmittance of the ZnO-P(VDF-TrFE) layer displayed a similar transparency to that of the ZnO ETL alone as shown in Figure 1d, which indicates that there will be negligible light loss and performance degradation because of the addition of the P(VDF-TrFE) layer.

Cross-sectional illustrations describing the effect of modulation of the piezoelectric potential on the flexible PbS QDSCs are shown in **Figure 2** along with 3D plan views of a porous P(VDF-TrFE) layer, which are also shown in Figure S2a,b (Supporting Information). In addition, the evolution of the morphology following deposition of a QD layer on the porous P(VDF-TrFE) structure was recorded using an AFM, which revealed that the porous structure became fully filled with QDs as shown in Figure S3 (Supporting Information). As revealed by X-ray diffraction (XRD) measurements in Figure 1c, a β-phase P(VDF-TrFE) layer exhibits a certain molecular orientation (Figure S2c, Supporting Information) in such a way that negative fluorine (F) atoms align to one side of the backbone and positive hydrogen atoms align to the other side. As a result, a P(VDF-TrFE) layer exhibits a spontaneous polarization.[27,28] When the spatially symmetrical arrangement of a β-crystalline P(VDF-TrFE) backbone chain becomes asymmetry through the application of strain, the induced polarization of the P(VDF-TrFE) increases (or decreases) because the magnitude of the polarization is proportional to the distance between the F and H atoms.[27,29] This structural change in the P(VDF-TrFE) molecules causes the magnitude of the piezoelectric potential to be modulated by the application of mechanical stress/strain as shown in Figure S2d,e (Supporting Information), which in turn enables the behavior of the charge carriers in a flexible QDSC to be modulated.

As shown in Figure 2a,b, the application of a compressive strain to the flexible PbS QDSC induces a piezoelectric potential, which leads to the formation of a steep electric potential, i.e., higher electric field, at the junction as a result of the modulation of the space charge region compared to a QDSC that is not subjected to any strain (no strain). Consequently, exciton dissociation and charge carrier extraction are enhanced at the heterojunction. On the contrary, exciton dissociation and charge carrier extraction are diminished when a gradual distribution of the electric potential, i.e., lower electric field, was formed at the junction under tensile strain as shown in Figure 2c.

In order to understand the changes in the junction properties, such as the distribution of the electric potential and the space charge region at the heterojunction that results from the piezoelectric potential under the application of strain, we carried out simulations with the COMSOL Multiphysics software. It is worth noting that a ZnO layer which was spin-coated from a solution phase did not exhibit a piezoelectric potential as shown in Figure S1c (Supporting Information) due to the random orientation of the ZnO nanoparticles and thus only a porous P(VDF-TrFE) layer was chosen as the piezoelectric material for the simulation. Details of the parameters and equations used for the simulations are described in Section I of the Supporting Information. As shown in **Figure 3**a, the distribution

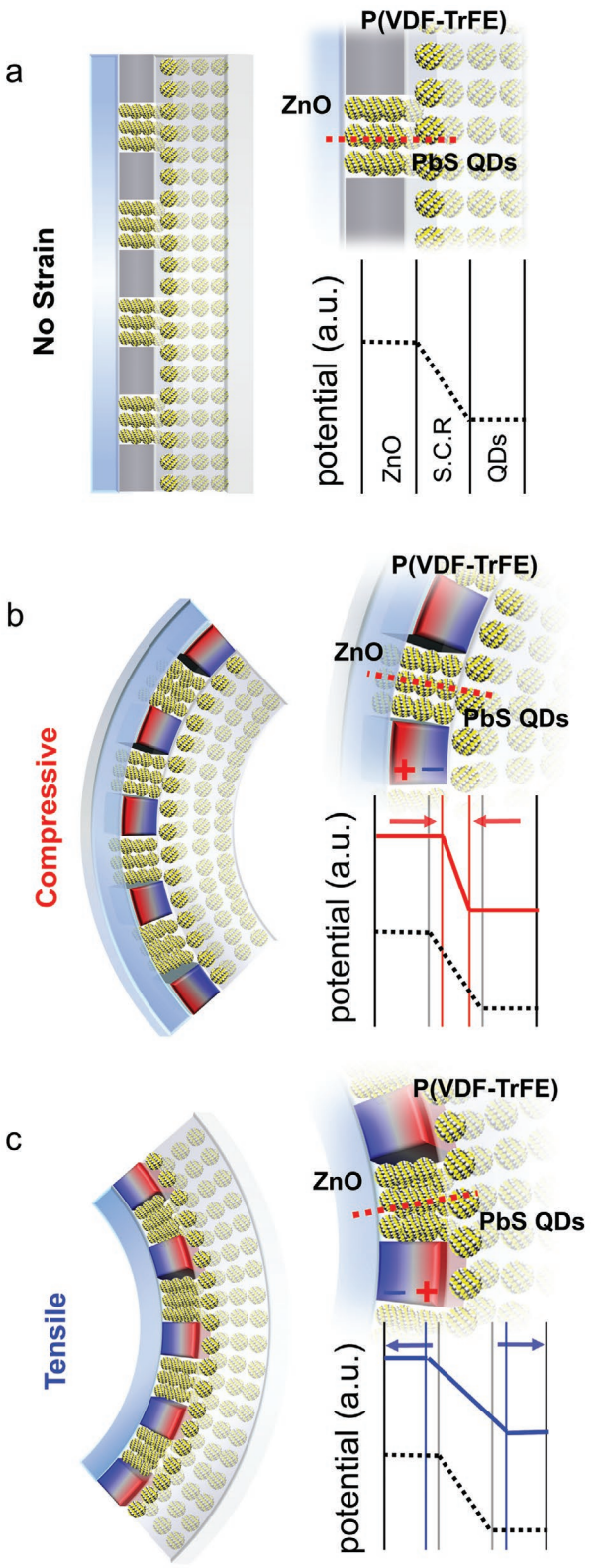

Figure 2. Illustration highlighting the modulation of the junction properties through changes in the piezoelectric potential in the flexible PbS QDSC a) with no strain and upon the application of b) a compressive and c) a tensile strain, where S.C.R. indicates the space charge region and the red dotted line indicates the line on which the potential profile is read.

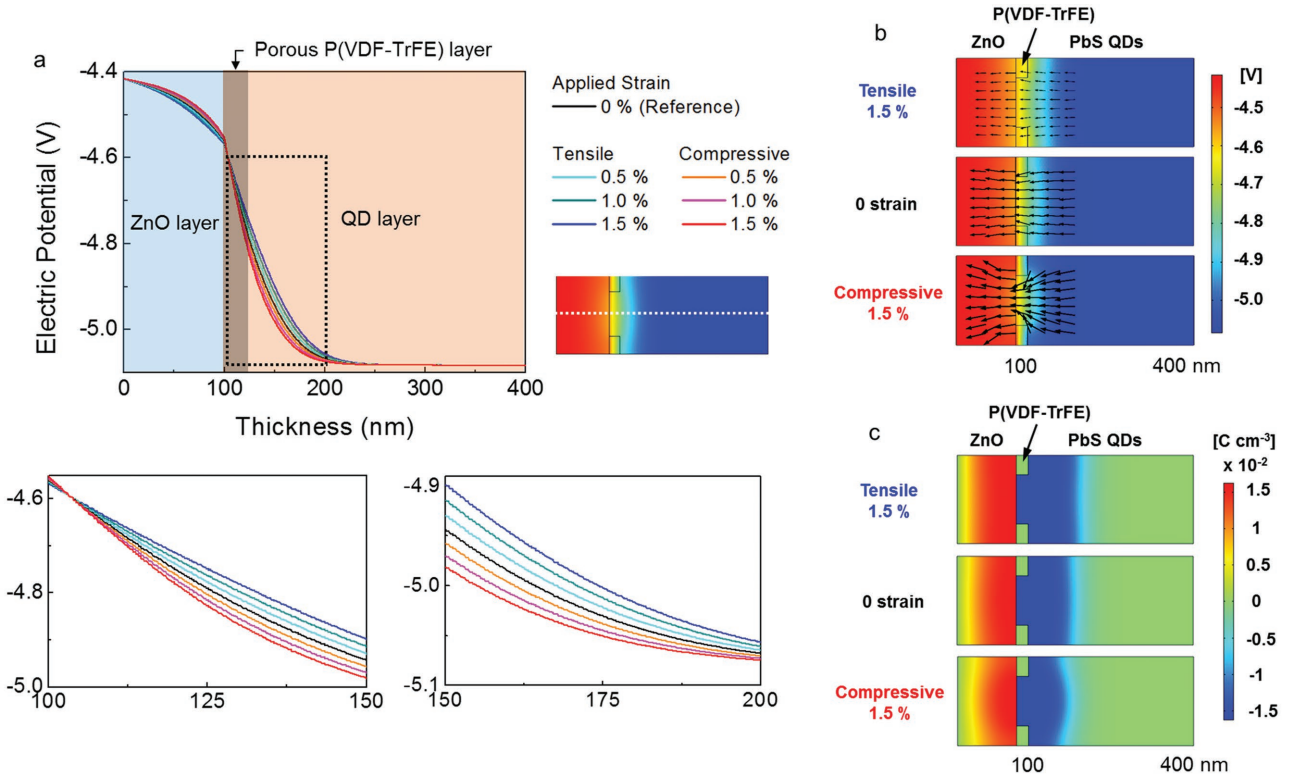

Figure 3. a) Cross-sectional view of the distribution of the electric potential at the ZnO-PbS QD heterojunction, where the potential over the region from 100 to 200 nm was enlarged in the lower plots; the potential was read at the position as indicated by the white dotted line for different applied strain amplitudes. b) 2D distribution of the electric potential at the junction for 1.5% tensile, 0 and 1.5% compressive strain, respectively. The arrows indicate the direction of electron flow and the size of the arrows indicates the intensity of the electric field at that point. c) 2D representation of the space charge region for 1.5% tensile, 0 and 1.5% compressive strain, respectively, where the red color describes a density of positively bound charges and the blue color a density of negatively bound charges.

of the electric potential across the ZnO-PbS QD layers can be modulated by the application of compressive and tensile strain. The slope of the electric potential distribution across the junction became steeper when the compressive strain was applied to the devices, which enhanced exciton dissociation and charge extraction. On the other hand, the application of tensile strain resulted in a gradual electric potential distribution at the junction and consequently exciton dissociation and charge extraction were decreased. Further, the enhanced electric field introduced by the strain (no strain to compressive 1.5%) at the heterojunction (100–120 nm) was ≈33% (from 7.5×10^6 (no strain) to 10^7 V m^{-1} (compressive 1.5%)).

The color changes at the heterojunction in Figure 3b highlight the modulation of the electric potential due to the application of compressive and tensile strains. Under compressive strain, charge carriers were drawn into the pores in the P(VDF-TrFE) layer and were effectively transported to the ZnO layer as described by the direction of the arrows. By contrast, it was observed that the formation of the diverging and weak distribution of the electric potential for a tensile strain could not effectively transport photogenerated charges to the ZnO layer as shown in Figure 3b, which led to severe charge carrier loss at the heterojunction. Also, the size of the arrows, which are proportional to the amplitude of the electric field at each point, describes the modulation of the electric potential/field by compressive and tensile strain. This modulation of the electric potential/field is also attributed to the modulation of the space charge region by the induced piezoelectric potential as shown in Figure 3c, where colored regions of red and blue indicate the density of positive and negative space charges, respectively. The formation of a narrow space charge region resulted in the generation of a steep distribution in the electric potential at the heterojunction, whereas the formation of a wide space charge region ended up with the generation of a gradual potential change as illustrated in Figure 3b (Equation (1) for potential distribution at semiconducting junction in Section II of the Supporting Information). The simulation results highlight that the modulated piezoelectric potential that is caused by simply changing the directions of the strain imposed on the piezoelectric layer is able to modulate the space charge region and also the potential distribution, which can facilitate or hinder the transport of charge carriers.

Experimental verification of the modulation in the charge carrier transport that is caused by the piezoelectric potential was then carried out by fabricating flexible QDSCs with the structure presented in Figure 1a. As shown in **Figure 4**a, it is evident that the P(VDF-TrFE) layer without the porous structure restricted the transport of photogenerated charge carriers due to the insulating nature of the P(VDF-TrFE) layer, which resulted in a poor solar cell performance compared to that of the flexible QDSC with a porous P(VDF-TrFE) layer (Table S1,

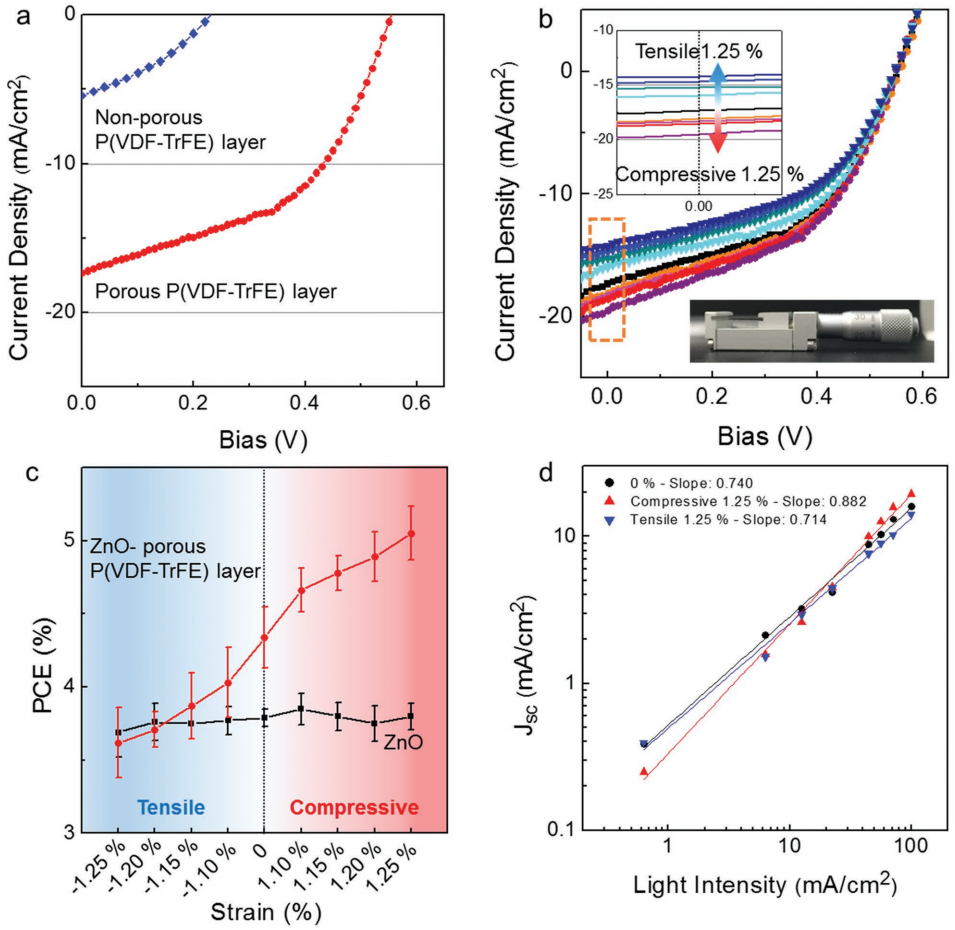

Figure 4. a) Performance of the flexible QDSC measured in the absence of any strain where the blue curve is for the ZnO-P(VDF-TrFE) sample without a porous polymer structure and the red curve represents the ZnO-P(VDF-TrFE) sample with a porous structure. b) *J–V* curves at no strain as well as compressive and tensile strain ranging from 1.10 to 1.25%; top left inset shows enlarged J_{sc} level for different strain amplitudes, and bottom right inset shows the bending machine with a micrometer. c) Modulation of the power conversion efficiency of the ZnO-P(VDF-TrFE) layer with a porous structure (red) and the QDSC with only a ZnO layer (black) with respect to the application of a tensile and compressive strain. d) Dependence of the short circuit current, J_{sc}, on the light intensity for 0, 1.25% compressive, and 1.25% tensile strain. The solid lines are linear fits to the data.

Supporting Information). The thicknesses of both P(VDF-TrFE) layers were ≈20 nm and the porous structures were fabricated by controlling the evaporation rate as well as the concentration of the P(VDF-TrFE) solution as shown in Figure S4 (Supporting Information). The performances of QDSCs with a porous P(VDF-TrFE) layer were optimized and the optimized conditions were used for all QDSCs unless otherwise stated as shown in Figure S5 and Table S2 (Supporting Information). More details about the fabrication of a porous structure P(VDF-TrFE) layer are described in the Experimental Section. It is noted that the enhanced performance of the flexible QDSC with a porous P(VDF-TrFE) layer compared to the QDSC with only a ZnO layer at no applied strain in Figure 4c (0 strain column) is due to the spontaneous polarization of the electric dipoles in the P(VDF-TrFE), which was repeatedly observed in PbS QDSCs based on a glass substrate that prohibits any strain as shown in Figure S6 and Table S3 (Supporting Information).[18] This result emphasizes that the porous P(VDF-TrFE) layer facilitates charge carrier transport and improves the performance of a QDSC via the piezoelectric effect; without this effect the layer would severely deteriorate the performance due to the insulating nature of the polymer.

The effect of the piezoelectric potential on the solar cell performance was investigated by applying compressive or tensile strain to the flexible QDSCs with the porous P(VDF-TrFE) layer. The applied strain was carefully controlled by a micrometer that was attached to a bending machine as shown in the bottom inset of Figure 4b. A noticeable modulation in J_{sc}, on the order of ≈37% (from 14.18 to 19.53 mA cm^{-2}), was observed at various strain rates as shown in Figure 4b and Table S1 (Supporting Information). This is attributed to an increase (or decrease) in the exciton dissociation and charge extraction as the applied electric potential at the junction was increased (decreased) by the application of larger compressive (or tensile) strain as illustrated in Figure 3. Also, it was observed that the performance of the solar cell was maintained under repeated strain that was applied by changing the direction of strain, compressive to tensile or tensile to compressive, as shown in Figure S7 (Supporting Information). The experimental result was consistent with the theoretical simulations,

which predicted a modulation of the J_{sc} (performed using the COMSOL Multiphysics software) as shown in Figure S8 (Supporting Information) and also in the equation for the exciton dissociation rates as a function of the applied electric potential in Section II of the Supporting Information.[24,30] However, a modulation of V_{oc} was not noticeable compared to that observed for J_{sc} because the induced piezoelectric potential was effective only on the heterojunction and adjacent area, and did not affect the quasi-Fermi level of the whole solar cell system. A similar phenomenon was also observed in solar cells that exploited ferroelectricity.[31] As a result of the J_{sc} modulation, the PCE values were also found to be substantially altered, for example, ΔPCE ≈ 1.37% (from 3.68% to 5.05%), as depicted in Figure 4c (red), which indicates that the performance of the solar cell is controllable by simply adjusting the strain rates applied to the flexible QDSC. However, for the QDSC with only a ZnO layer (i.e., without the presence of a piezoelectric effect) there was a negligible change in the performance when either compressive or tensile strain was applied, as shown in Figure 4c (black) and Figure S9 and Table S4 (Supporting Information). It is worth stressing that the applied strain was kept relatively low (up to 1.25%) and thus the maximum change in distance between the QDSC and the light source was 2.5 mm which is a small change considering that a solar simulator is a collimated light source. A stark difference in the modulation of the PCE in two types of QDSCs (Figure 4c) suggests that the small distance change that arises through a bending of the QDSCs had a negligible effect on the performance enhancement, which supports our finding that the modulation of the charge carrier behavior and the distribution of the potential at the heterojunction was caused by a piezoelectric effect of the porous P(VDF-TrFE) layer. The average values for the parameters from 15 separate flexible QDSCs are shown in **Table 1**. When a higher strain was applied, however, we observed degradation in the solar cell performance, which was due to the formation of cracks on the QD films as demonstrated in Figure S10 and Table S5 (Supporting Information). The strain rate was calculated based on the assumption that the applied strain is approximately equal to the strain of the outer surface of the flexible substrates because the thickness of the substrate (0.2 mm) is much larger than the total thickness of the QDSCs (500 nm).[32,33] The QDSCs with only a ZnO layer and with a ZnO-porous P(VDF-TrFE) layer showed reliable long-term stability under the application of mechanical vibrations with a linear motor (Figure S1, Supporting Information), which is the similar effect as straining the QDSC, for 2 h (more than 210 000 cycles) as shown in Figure S11 and Table S6 (Supporting Information).

The efficient charge dissociation and extraction in the flexible QDSCs is also ascribed to the improved recombination kinetics, which were investigated by considering the dependence of the solar cell performance on the light intensity as well as the calculation of the ideality factor. As shown in Figure 4d, the exponential factor α that was calculated from a linear fit to J_{sc} as a function of light intensity on a logarithmic scale ($J_{sc} \propto I^{\alpha}$, where I is light intensity) shows clearly different aspects of the recombination dynamics. When compressive strain was applied to the QDSC the slope approached unity in contrast to that observed for no strain or tensile strain, which indicates that charge carriers are effectively transported prior to recombination, i.e., reduced nonradiative recombination.[34,35] Also, the calculated ideality factor was consistent with the result of the light intensity dependent solar cell performance. Upon the application of compressive strain on the QDSC, nonradiative recombination was suppressed whereas the opposite trend was observed with tensile strain as shown in Table S8 (Supporting Information).[36–38] Ideality factors were calculated using Equation (3) in Section II of the Supporting Information and the dark saturation current shown in Figure S12 (Supporting Information). Complementary results for the recombination dynamics revealed that the application of compressive strain led to improved charge carrier transport and reduced charge carrier loss, which resulted in the suppression of nonradiative recombination and thus an improvement of the overall flexible QDSC performance.

In summary, we have shown that the implementation of a piezoelectric polymer P(VDF-TrFE) layer with a porous structure on top of the ZnO layer in a flexible QDSC can result in an enhancement of the overall solar cell performance when subjected to compressive strain. Using a separate P(VDF-TrFE) film ensures that the semiconducting properties of the ZnO and PbS QD layers are retained, which could otherwise be degraded through the formation of conjugated structures such as a semiconducting ETL with P(VDF-TrFE). In

Table 1. Average value of the solar cell parameters taken from 15 separate devices at 1.25% compressive, 0, and 1.25% tensile strain as shown in Figure 4c.

Sample	Strain [%]	V_{oc} [V]	J_{sc} [mA cm^{-2}]	FF	PCE [%]
Figure 4c	Compressive 1.25	0.55 ± 0.0101	19.53 ± 0.7168	0.47 ± 0.0170	5.05 ± 0.1840
	Compressive 1.20	0.55 ± 0.0092	18.68 ± 0.3226	0.48 ± 0.0189	4.91 ± 0.1696
	Compressive 1.15	0.55 ± 0.01	18.23 ± 0.3830	0.48 ± 0.0140	4.80 ± 0.1184
	Compressive 1.10	0.55 ± 0.01	17.79 ± 0.2548	0.48 ± 0.0192	4.68 ± 0.1496
	0	0.55 ± 0.0074	17.40 ± 0.3274	0.47 ± 0.0250	4.50 ± 0.2076
	Tensile 1.10	0.55 ± 0.01	15.84 ± 0.4364	0.47 ± 0.0210	4.09 ± 0.2392
	Tensile 1.15	0.55 ± 0.0095	15.28 ± 0.2328	0.47 ± 0.0158	3.95 ± 0.2264
	Tensile 1.20	0.55 ± 0.0074	14.77 ± 0.2682	0.47 ± 0.0155	3.80 ± 0.1228
	Tensile 1.25	0.55 ± 0.0079	14.18 ± 0.3310	0.47 ± 0.0190	3.68 ± 0.2424

accordance with the simulations, the piezoelectric potential that was generated by the strain/stress was found to increase the electric potential/field at the ZnO-PbS QD heterojunction due to a modulation of the space charge region. In addition, the performance of the flexible PbS QDSCs could be actively modulated by simply applying various strain rates, which is attributed to the enhanced exciton dissociation, charge extraction, and reduced trap-assisted recombination. Using this approach, an increase of the power conversion efficiency of ≈37% was demonstrated.

Experimental Section

Solar Cell Fabrication: Colloidal PbS QDs and ZnO nanoparticle solution were synthesized according to previously reported methods.[39] For the ZnO ETL layer, a solution of ZnO nanoparticles in chloroform was spin-coated onto patterned indium tin oxide (ITO) that was either coated onto flexible or glass substrates at 3000 rpm for 40 s and thermally annealed at 130 °C for 2 h in an oven. For the ZnO-P(VDF-TrFE) ETL layer, an additional solution of 0.5–1 wt% P(VDF-TrFE) was spin-coated on to the ZnO film at 3000–4000 rpm for 30 s and then thermally annealed at the same experimental conditions. 2-Butanon, which was chosen as it has a relatively low boiling point that is advantageous for drying the solvent quickly, was used as a solvent for dissolving P(VDF-TrFE). Various spin-coating speeds were used from 3000 to 5000 rpm and the optimized conditions were obtained for a concentration of 0.5 wt% with a spin-coating speed of 3000 rpm. Afterward, PbS QD layers were spin-coated at 2500 rpm. For the solid-state ligand exchange of the PbS QD layers, a TBAI solution with a concentration of 10 mg mL^{-1} was loaded and held for 30 s, which was followed by a washing process with methanol. EDT treated QD layer (0.02 vol% in acetonitrile) was prepared by the same procedure as the TBAI except that acetonitrile was used as the solvent for the washing procedure. All QDSCs consisted of 10 layers of TBAI and 2 layers of EDT structures, unless stated otherwise. Gold electrodes with 100 nm thickness were deposited using thermal evaporation.

Solar Cell Characterization: Solar cell measurements were performed using a source meter (Keithley 4200-SCS) and a solar simulator (LOT-Quantum Design) with an AM 1.5 G filter (100 mW cm^{-2}). The standard cell (Rera system) was measured before solar cell measurements. All measurements were carried out in ambient air at room temperature. To specify the size of the active area, we used a mask pattern with a size of 0.018 ± 0.001 cm^2.

Supporting Information

Supporting Information is available from the Wiley Online Library or from the author.

Acknowledgements

This work was supported by the International Collaborative Energy Technology R&D Program of the Korea Institute of Energy Technology Evaluation and Planning (KETEP), and was granted financial resource from the Ministry of Trade, Industry & Energy, Republic of Korea (20142020103970), National Research Foundation (NRF) of Korea (2015M2A2A6A02045252), and the European Research Council under ERC Grant Agreement n. 340538.

Conflict of Interest

The authors declare no conflict of interest.

Keywords

charge transport modulation, flexible solar cells, lead sulfide quantum dots, piezoelectric effect

Received: March 24, 2017
Revised: July 11, 2017
Published online: September 22, 2017

[1] M. Kaltenbrunner, M. S. White, E. D. Głowacki, T. Sekitani, T. Someya, N. S. Sariciftci, S. Bauer, *Nat. Commun.* **2012**, *3*, 770.
[2] K. Li, H. Zhen, L. Niu, X. Fang, Y. Zhang, R. Guo, Y. Yu, F. Yan, H. Li, Z. Zheng, *Adv. Mater.* **2014**, *26*, 7271.
[3] J. Nam, Y. Lee, W. Choi, C. S. Kim, H. Kim, J. Kim, D. Kim, S. Jo, *Adv. Energy Mater.* **2016**, *6*, 1601269.
[4] Q. Lin, L. Lu, M. M. Tavakoli, C. Zhang, G. C. Lui, Z. Chen, X. Chen, L. Tang, D. Zhang, Y. Lin, *Nano Energy* **2016**, *22*, 539.
[5] J. H. Heo, M. H. Lee, H. J. Han, B. R. Patil, J. S. Yu, S. H. Im, *J. Mater. Chem. A* **2016**, *4*, 1572.
[6] S. Savagatrup, A. D. Printz, T. F. O'Connor, A. V. Zaretski, D. Rodriquez, E. J. Sawyer, K. M. Rajan, R. I. Acosta, S. E. Root, D. J. Lipomi, *Energy Environ. Sci.* **2015**, *8*, 55.
[7] J. Ham, W. J. Dong, J. Y. Park, C. J. Yoo, I. Lee, J. Lee, *Adv. Mater.* **2015**, *27*, 4027.
[8] K. Poorkazem, D. Liu, T. L. Kelly, *J. Mater. Chem. A* **2015**, *3*, 9241.
[9] I. J. Kramer, G. Moreno-Bautista, J. C. Minor, D. Kopilovic, E. H. Sargent, *Appl. Phys. Lett.* **2014**, *105*, 163902.
[10] Y. Li, L. Wei, C. Wu, C. Liu, Y. Chen, H. Liu, J. Jiao, L. Mei, *J. Mater. Chem. A* **2014**, *37*, 15546.
[11] F. W. Wise, *Acc. Chem. Res.* **2000**, *33*, 773.
[12] X. Lan, O. Voznyy, F. P. García de Arquer, M. Liu, J. Xu, A. H. Proppe, G. Walters, F. Fan, H. Tan, M. Liu, Z. Yang, S. Hoogland, E. H. Sargent, *Nano Lett.* **2016**, *16*, 4630.
[13] B. Kim, D. C. Neo, B. Hou, J. B. Park, Y. Cho, N. Zhang, J. Hong, S. Pak, S. Lee, J. I. Sohn, *ACS Appl. Mater. Interfaces* **2016**, *8*, 13902.
[14] G. W. Hwang, D. Kim, J. M. Cordero, M. W. Wilson, C. M. Chuang, J. C. Grossman, M. G. Bawendi, *Adv. Mater.* **2015**, *27*, 4481.
[15] C. M. Chuang, A. Maurano, R. E. Brandt, G. W. Hwang, J. Jean, T. Buonassisi, V. Bulović, M. G. Bawendi, *Nano Lett.* **2015**, *15*, 3286.
[16] J. Hong, B. Hou, J. Lim, S. Pak, B.-S. Kim, Y. Cho, J. Lee, Y.-W. Lee, P. Giraud, S. Lee, J. B. Park, S. M. Morris, H. J. Snaith, J. I. Sohn, S. Cha, J. M. Kim, *J. Mater. Chem. A* **2016**, *4*, 18769.
[17] R. Azmi, S. Oh, S. Jang, *ACS Energy Lett.* **2016**, *1*, 100.
[18] G. Kim, F. P. García de Arquer, Y. J. Yoon, X. Lan, M. Liu, O. Voznyy, Z. Yang, F. Fan, A. H. Ip, P. Kanjanaboos, S. Hoogland, J. Y. Kim, E. H. Sargent, *Nano Lett.* **2015**, *15*, 7691.
[19] P. H. Rekemeyer, S. Chang, C. M. Chuang, G. W. Hwang, M. G. Bawendi, S. Gradečak, *Adv. Energy Mater.* **2016**, *6*, 1600848.
[20] X. Zhang, E. M. Johansson, *J. Mater. Chem. A* **2017**, *5*, 303.
[21] C. H. Chuang, P. R. Brown, V. Bulovic, M. G. Bawendi, *Nat. Mater.* **2014**, *13*, 796.
[22] K. Shin, T. Y. Kim, G. C. Yoon, M. K. Gupta, S. K. Kim, W. Seung, H. Kim, S. Kim, S. Kim, S. Kim, *Adv. Mater.* **2014**, *27*, 5619.
[23] S. B. Jo, M. Kim, D. H. Sin, J. Lee, H. G. Kim, H. Ko, K. Cho, *Adv. Energy Mater.* **2015**, *5*, 1500802.
[24] K. S. Nalwa, J. A. Carr, R. C. Mahadevapuram, H. K. Kodali, S. Bose, Y. Chen, J. W. Petrich, B. Ganapathysubramanian, S. Chaudhary, *Energy Environ. Sci.* **2012**, *5*, 7042.
[25] Y. Cho, J. B. Park, B. Kim, J. Lee, W. Hong, I. Park, J. E. Jang, J. I. Sohn, S. Cha, J. M. Kim, *Nano Energy* **2015**, *16*, 524.
[26] G. Ni, Y. Zheng, S. Bae, C. Y. Tan, O. Kahya, J. Wu, B. H. Hong, K. Yao, B. Ozyilmaz, *ACS Nano* **2012**, *6*, 3935.

[27] J. Lee, K. Y. Lee, B. Kumar, N. T. Tien, N. Lee, S. Kim, *Energy Environ. Sci.* **2013**, *6*, 169.
[28] J. Lee, K. Y. Lee, M. K. Gupta, T. Y. Kim, D. Lee, J. Oh, C. Ryu, W. J. Yoo, C. Kang, S. Yoon, *Adv. Mater.* **2014**, *26*, 765.
[29] K. S. Ramadan, D. Sameoto, S. Evoy, *Smart Mater. Struct.* **2014**, *23*, 033001.
[30] Y. Yuan, T. J. Reece, P. Sharma, S. Poddar, S. Ducharme, A. Gruverman, Y. Yang, J. Huang, *Nat. Mater.* **2011**, *10*, 296.
[31] S. Nam, J. Seo, S. Woo, W. H. Kim, H. Kim, D. D. Bradley, Y. Kim, *Nat. Commun.* **2015**, *6*, 8929.
[32] S. Liu, Q. Liao, S. Lu, Z. Zhang, G. Zhang, Y. Zhang, *Adv. Funct. Mater.* **2016**, *26*, 1347.
[33] R. Yang, Y. Qin, L. Dai, Z. L. Wang, *Nat. Nanotechnol.* **2009**, *4*, 34.
[34] D. Zhao, M. Sexton, H.-Y. Park, G. Baure, J. C. Nino, F. So, *Adv. Energy Mater.* **2015**, *5*, 1401855.
[35] H. Aqoma, N. Barange, I. Ryu, S. Yim, Y. R. Do, S. Cho, D. Ko, S. Jang, *Adv. Funct. Mater.* **2015**, *25*, 6241.
[36] D. Bozyigit, W. M. Lin, N. Yazdani, O. Yarema, V. Wood, *Nat. Commun.* **2015**, *6*, 6180.
[37] W. Yoon, J. E. Boercker, M. P. Lumb, D. Placencia, E. E. Foos, J. G. Tischler, *Sci. Rep.* **2013**, *3*, 2225.
[38] D. Zhitomirsky, O. Voznyy, L. Levina, S. Hoogland, K. W. Kemp, A. H. Ip, S. M. Thon, E. H. Sargent, *Nat. Commun.* **2014**, *5*, 3803.
[39] B. Hou, Y. Cho, B. S. Kim, J. Hong, J. B. Park, S. J. Ahn, J. I. Sohn, S. Cha, J. M. Kim, *ACS Energy Lett.* **2016**, *1*, 834.